

## Article

# Numerical Simulation and Field Experimental Study of Combustion Characteristics of Hydrogen-Enriched Natural Gas

Chen Sun <sup>1,†</sup>, Tiantian Wang <sup>2,†</sup>, Pengtao Wang <sup>1</sup>, Yi Zhang <sup>3</sup>, Chong Cui <sup>1</sup>, Yanghui Lu <sup>1,\*</sup>, Wei Liu <sup>1</sup>, Yangxin Zhang <sup>3,\*</sup> and Yang Zhang <sup>3</sup>

<sup>1</sup> State Power Investment Corporation Research Institute Co., Ltd. (SPICRI), Beijing 102209, China

<sup>2</sup> Department of Energy and Power Engineering, Tsinghua University, Beijing 100084, China

<sup>3</sup> Shanxi Research Institute for Clean Energy, Tsinghua University, Taiyuan 030032, China

\* Correspondence: luyanghui@spic.com.cn (Y.L.); zhangyx@sice-tsinghua.org (Y.Z.)

† These authors contributed equally to this work.

**Abstract:** For the safe and efficient utilization of hydrogen-enriched natural gas combustion in industrial gas-fired boilers, the present study adopted a combination of numerical simulation and field tests to investigate its adaptability. Firstly, the combustion characteristics of hydrogen-enriched natural gas with different hydrogen blending ratios and equivalence ratios were evaluated by using the Chemkin Pro platform. Secondly, a field experimental study was carried out based on the WNS2-1.25-Q gas-fired boiler to investigate the boiler's thermal efficiency, heat loss, and pollutant emissions after hydrogen addition. The results show that at the same equivalence ratio, with the hydrogen blending ratio increasing from 0% to 25%, the laminar flame propagation speed of the fuel increases, the extinction strain rate rises, and the combustion limit expands. The laminar flame propagation speed of premixed methane/air gas reaches the maximum value when the equivalence ratio is 1.0, and the combustion intensity of the flame is the highest at this time. In the field tests, as the hydrogen blending ratio increases from 0% to nearly 10% with the increasing excess air ratio, the boiler's thermal efficiency decreases as well as the NO<sub>x</sub> emission. This indicates that there exists a tradeoff between the boiler thermal efficiency and NO<sub>x</sub> emission in practice.

**Keywords:** hydrogen-enriched natural gas; combustion characteristics; field tests; numerical simulation



**Citation:** Sun, C.; Wang, T.; Wang, P.; Zhang, Y.; Cui, C.; Lu, Y.; Liu, W.; Zhang, Y.; Zhang, Y. Numerical Simulation and Field Experimental Study of Combustion Characteristics of Hydrogen-Enriched Natural Gas.

*Processes* **2024**, *12*, 1325.

<https://doi.org/10.3390/pr12071325>

Academic Editor: Adam Smoliński

Received: 9 April 2024

Revised: 1 May 2024

Accepted: 10 May 2024

Published: 26 June 2024



**Copyright:** © 2024 by the authors. Licensee MDPI, Basel, Switzerland. This article is an open access article distributed under the terms and conditions of the Creative Commons Attribution (CC BY) license (<https://creativecommons.org/licenses/by/4.0/>).

## 1. Introduction

Hydrogen, as a renewable energy source, has the advantages of low carbon emissions, high mass heat value, high energy density, and fast flame propagation speed. In industrial applications, it can promote the transformation of high energy-consuming and high-emission industries toward becoming green and low-carbon and is one of the clean energy sources with great development potential worldwide. As key equipment in industrial production, gas-fired boilers can accelerate flame propagation speed and increase flame temperature by blending hydrogen into natural gas, but it may cause an increase in NO<sub>x</sub> emissions from gas-fired boilers. Due to the increasingly stringent requirements for NO<sub>x</sub> emissions from combustion processes in China in recent years [1], the existing research on hydrogen-enriched natural gas combustion in industrial burners can no longer meet the latest NO<sub>x</sub> emission requirements. Therefore, to solve the problem of combustion and the utilization of hydrogen-enriched natural gas in gas-fired equipment, there is an urgent need to investigate safe, stable, and ultra-low NO<sub>x</sub> emission industrial boiler burner technologies and equipment [2].

Hydrogen addition changes the physicochemical properties of natural gas, especially in terms of the density [3], higher and lower heat value [4], etc. At present, domestic and foreign researchers have explored the effects of different hydrogen blending ratios on the combustion characteristics of hydrogen-enriched natural gas, mainly focusing on the flame propagation characteristics [5,6], combustion limits [7], combustion stability [8], and so on.

Hu et al. [9] analyzed the variation in the laminar flame propagation speed of hydrogen-enriched fuel under different operating conditions using a fixed-capacity combustion bomb experimental platform, and the results showed that increasing the proportion of hydrogen accelerates the laminar flame propagation speed. Ghosh et al. [10] found that the minimum ignition energy and the flameout distance decreased with increasing hydrogen content. Colorado et al. [11] explored the effect of different hydrogen blending ratios on the flashback characteristics, and their experimental study showed that no flashback occurred in the premixed combustion burner when the hydrogen blending ratio was less than 30%. Griebel et al. [12] compared the blowout limits of hydrogen-enriched methane/air flames and found that hydrogen addition elevated the flame extinction limit, thus helping to improve the ability of the flame to maintain stable combustion under near-limit conditions.

In addition, as shown in Table 1, some researchers have also investigated the combustion characteristics of hydrogen-enriched natural gas applied to gas-fired boilers and explored the effects of the hydrogen blending ratio on boiler energy efficiency [13] and pollutant emission characteristics through experiments [14,15], computational fluid dynamic (CFD) simulation [16], chemical reaction network (CRN) simulation [17], and modeling studies [18]. For condensing gas-fired boilers, with a constant heating load, the mass of condensable water in the flue gas increases as the hydrogen proportion in the fuel increases, which contributes to improving the condensing efficiency of the boiler [19]. In the case of non-condensing gas-fired boilers, an increase in the hydrogen blending ratio can lead to an increase in the thermal efficiency of the boiler, if the boiler's operating parameters are adjusted to try to keep the flue gas temperature as consistent as possible without changing the excess air ratio [20]. Some studies [21,22] have analyzed the results of CFD modeling and pointed out that at a constant equivalence ratio, the increase in the hydrogen blending ratio would increase the thermal NO<sub>x</sub> emission in the boiler. Jones et al. [23] pointed out that hydrogen addition expanded the lean burn limit of the fuel, and by decreasing the equivalence ratio, the combustion was pushed to a leaner burn state, which could reduce the NO<sub>x</sub> emissions from the boiler.

**Table 1.** A brief summary of hydrogen-enriched natural gas-fired boilers.

Authors	Methods	Focuses	Ref.
Lo Basso et al.	Thermodynamic modeling	Efficiency and carbon emissions	[13]
Hoelzner et al.	Boiler experiments	Efficiency and NO <sub>x</sub> emission	[14]
Ding et al.	Burner experiments	Equivalence ratio control	[15]
Öztuna et al.	CFD simulation	NO <sub>x</sub> and carbon emissions	[16]
Wang et al.	CRN simulation	Efficiency and NO <sub>x</sub> emission	[17]
Schiro et al.	Thermodynamic modeling	Efficiency and carbon emissions	[18,19]
Bălănescu et al.	Thermodynamic modeling	Efficiency and carbon emissions	[20]
Cellek et al.	CFD simulation	NO <sub>x</sub> and carbon emissions	[21]
Büyükkakin et al.	CFD simulation	NO <sub>x</sub> and carbon emissions	[22]
Jones et al.	Theoretical modeling	Combustion stability and NO <sub>x</sub> emission	[23]

The aforementioned studies on hydrogen-enriched natural gas-fired boilers are mostly based on numerical simulation or modeling, while several experimental studies have mainly focused on burners and laboratory-grade boilers, with limited experimental research on the comprehensive consideration of combustion stability, pollutant emissions, and boiler thermal efficiency in hydrogen-enriched natural gas combustion in industrial boilers for practical applications. Therefore, in this study, a numerical simulation was conducted to investigate the combustion characteristics of hydrogen-enriched natural gas under different hydrogen blending ratios and equivalence ratios by using the Chemkin Pro 2019 R1 platform [24] integrated into Ansys software (Canonsburg, PA, USA) coupled with the FFCM-1 chemical kinetic mechanism [25], and this mechanism has been verified to better predict hydrogen-rich fuels [26]. Further, a 2 t/h gas-fired steam boiler (WNS2-1.25-Q) was utilized to carry out on-site hydrogen-enriched natural gas combustion tests, to investigate the impact of different hydrogen blending ratios and excess air ratios on the thermodynamic and combustion characteristics (e.g., boiler thermal efficiency, pollutant emissions, etc.)

of the industrial gas-fired boiler, and to verify the combustion stability of the boiler after hydrogen addition for a long period of continuous operation. The present study may shed light on the technological development of an industrial hydrogen-enriched natural gas-fired boiler with stable operation and low NO<sub>x</sub> combustion.

## 2. Combustion Characteristics of Hydrogen-Enriched Natural Gas

In this section, we discuss the chemical kinetics software Ansys Chemkin Pro that was utilized to numerically investigate the effects of the hydrogen blending ratio  $X_{H_2}$  on the laminar flame propagation speed  $S_L$ , extinction strain rate  $K_{ext}$ , and flammability limits of hydrogen-enriched natural gas. As we all know, methane is the main component of natural gas [27], and thus, methane is viewed as a substitute for natural gas in the numerical simulation to simplify the calculation. The hydrogen blending ratio  $X_{H_2}$  was calculated according to Equation (1):

$$X_{H_2} = \frac{V_{H_2}}{V_{H_2} + V_{CH_4}} \quad (1)$$

where  $V_{H_2}$  denotes the volume flow rate of hydrogen, m<sup>3</sup>/s;  $V_{CH_4}$  denotes the volume flow rates of methane, m<sup>3</sup>/s.

The physical properties of methane (CH<sub>4</sub>) and hydrogen (H<sub>2</sub>) are shown in Table 2. Among them, the lower heat value, Wobbe index, and density are the key physical parameters in this study. As for the hydrogen-enriched natural gas, the density and heat value both linearly decrease, while the Wobbe index first decreases and then slightly increases as the hydrogen blending ratio increases from 0% to 100%.

**Table 2.** Basic physical parameters of methane (CH<sub>4</sub>) and hydrogen (H<sub>2</sub>).

Parameters	CH <sub>4</sub>	H <sub>2</sub>
Molecular mass	16.04	2.02
Density/(kg/m <sup>3</sup> )	0.6709	0.0841
Constant-pressure specific heat capacity/(kJ/(kg·K))	2.210	14.268
Constant-volume specific heat capacity/(kJ/(kg·K))	1.686	10.141
Lower heat value/(MJ/m <sup>3</sup> )	34.04	10.23
Higher heat value/(MJ/m <sup>3</sup> )	37.77	12.07
Octane value	120	140
Relative density	0.5548	0.0695
Wobbe index/(MJ/m <sup>3</sup> )	50.71	45.78
Lewis number	0.99	0.33

The specific FFCM-1 chemical kinetic mechanism was used in this study. The component diffusion rate was calculated by using the multicomponent diffusion formula while considering the Soret diffusion effect. The adaptive grid calculation range was 10 cm, and the number of grids in the flame reaction area were 1000.

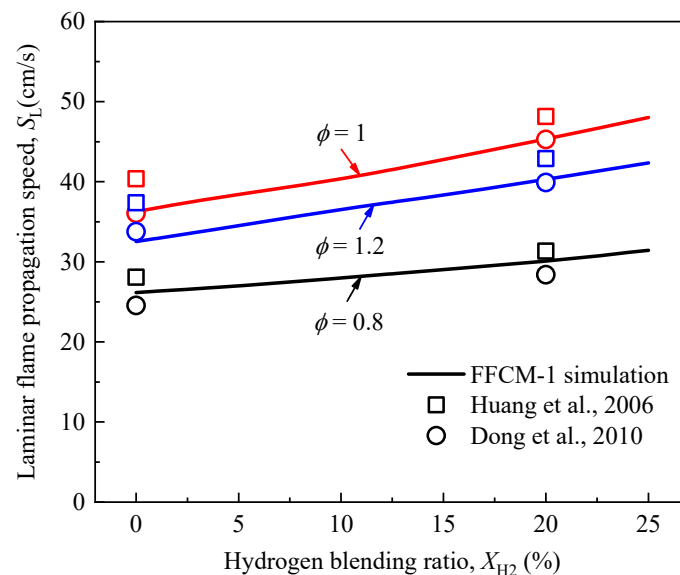
### 2.1. Laminar Flame Propagation Speed

The laminar flame propagation speed  $S_L$  was calculated using the one-dimensional premixed laminar flame model (PREMIX model) with the FFCM-1 chemical kinetic mechanism. Meanwhile, the calculated  $S_L$  was compared and verified with already published experimental data [5,6]. The comparison of parameters between Refs. [5,6] and the present study is listed in Table 3. The PREMIX model can be used to describe the premixed hydrogen-enriched natural gas flames of the constant-volume bomb and the Bunsen burner. In the present study, the values of initial temperature and pressure are nearly consistent with Refs. [5,6]. In addition, the ranges of the hydrogen blending ratio and equivalence ratio are also within the ranges of Refs. [5,6].

**Table 3.** A comparison of the parameters between the experimental studies and the present study.

Parameters	Ref. [5]	Ref. [6]	This Study
Methods	Constant-volume bomb	Bunsen burner	PREMIX model
Hydrogen blending ratio/(%)	0–100	0–100	0/5/10/15/20/25
Equivalence ratio	0.6–1.4	0.5–2.1	0.8/1.0/1.2
Initial pressure/(atm)	1	1	1
Initial temperature/(K)	300	293	293
Volumetric fraction of CH <sub>4</sub> in natural gas/(%)	96.16	--	100

Figure 1 shows the variation in the laminar flame propagation speed of hydrogen-enriched natural gas under different hydrogen blending ratios and equivalence ratios. It can be seen that as the hydrogen blending ratio increases from 0% to 25%, the laminar flame propagation speed monotonically increases by 20.18%, 32.41%, and 30.18%, respectively, and the equivalence ratio equals 0.8, 1.0, and 1.2. This indicates that the laminar flame propagation speed is more affected by hydrogen addition in fuel-rich combustion.

**Figure 1.** The variation in the laminar flame propagation speed of hydrogen-enriched natural gas with different hydrogen blending ratios and equivalence ratios [5,6].

In addition, the laminar flame propagation speed shows a trend of increasing and then decreasing as the equivalence ratio increases from 0.8 to 1.2. It is worth mentioning that the laminar flame propagation speed at  $\Phi = 1.0$  reaches the highest value compared to that at  $\Phi = 0.8$  and  $\Phi = 1.2$ . The laminar flame propagation speed at  $\Phi = 1.2$  is always higher than that at  $\Phi = 0.8$ , with the hydrogen blending ratio increasing from 0% to 25%.

## 2.2. Extinction Strain Rate

For a given combustion system, the blowout limit indicates the maximum combustible mixture velocity at which stable combustion can be maintained or the minimum combustible mixture velocity at which stable combustion can be disrupted. It is often characterized in terms of the extinction strain rate  $K_{ext}$  of the flame. The extinction strain rate  $K_{ext}$  was calculated using the quasi-one-dimensional counterflow premixed flame model (OPPDIF model) with the FFCM-1 chemical kinetic mechanism. Meanwhile, the calculated  $K_{ext}$  was also compared and verified with already published experimental data [26]. The comparison of parameters between Ref. [26] and the present study is listed in Table 4. The OPPDIF model can be used to describe the premixed hydrogen-enriched natural gas flames

on the counterflow flame burner. In the present study, the values of initial temperature and pressure are nearly consistent with Ref. [26]. In addition, the ranges of the hydrogen blending ratio and equivalence ratio are also within the ranges of Ref. [26].

**Table 4.** A comparison of the parameters between the experimental study and the present study.

Parameters	Ref. [26]	This Study
Methods	Counterflow flame burner	OPPDIF model
Hydrogen blending ratio/(%)	0–40	0/5/10/15/20/25
Equivalence ratio	0.7–1.3	0.8/1.0/1.2
Initial pressure/(atm)	1	1
Initial temperature/(K)	298	293
Volumetric fraction of CH <sub>4</sub> in natural gas/(%)	100	100

Figure 2 shows the variation in the extinction strain rate of hydrogen-enriched natural gas with different hydrogen blending ratios and equivalence ratios. As the hydrogen blending ratio increases from 0% to 25%, the extinction strain rate monotonically increases by 81.18%, 59.13%, and 50.86%, respectively, and the equivalence ratio equals 0.8, 1.0, and 1.2. This indicates that the extinction strain rate of the flame is more affected by hydrogen addition in fuel lean combustion. In addition, the increasing extinction strain rate implies that hydrogen addition helps to improve the combustion stability of the flame and the ability to maintain stable combustion under near-limit conditions.

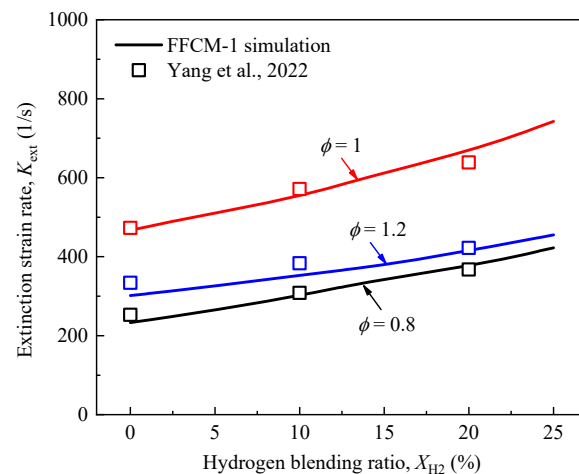


**Figure 2.** The variation in the extinction strain rate of hydrogen-enriched natural gas with different hydrogen blending ratios and equivalence ratios [26].

Moreover, the extinction strain rate of the flame shows a trend of increasing and then decreasing as the equivalence ratio increases from 0.8 to 1.2. Also, the extinction strain rate reaches the peak value when  $\Phi$  equals 1. The extinction strain rate of the flame at  $\Phi = 0.8$  is always lower than that at  $\Phi = 1.2$ , with the hydrogen blending ratio increasing from 0% to 25%.

### 2.3. Flammability Limits

Figure 3 demonstrates the variation in the flammability limits of hydrogen-enriched natural gas in the air as the hydrogen blending ratio increases from 0% to 100%. The flammability limits can be calculated according to Equation (2).

$$\frac{1}{L} = \sum \frac{X_k}{L_k} \quad (2)$$

Here,  $L$  denotes the upper or lower flammability limits in the air of hydrogen-enriched natural gas.  $L_k$  denotes the upper or lower flammability limits in the air of hydrogen and

methane, which are 4–75%, and 5–15%, respectively.  $X_k$  denotes the volumetric fraction of hydrogen and methane ( $\sum X_k = 1$ ).

It can be seen from Figure 3 that as the hydrogen blending ratio increases from 0% to 100%, the flammable range of hydrogen-enriched natural gas gradually expands, and the lower and upper flammability limits become closer and closer to the value of hydrogen (4–75%) and move away from the value of methane (5–15%).

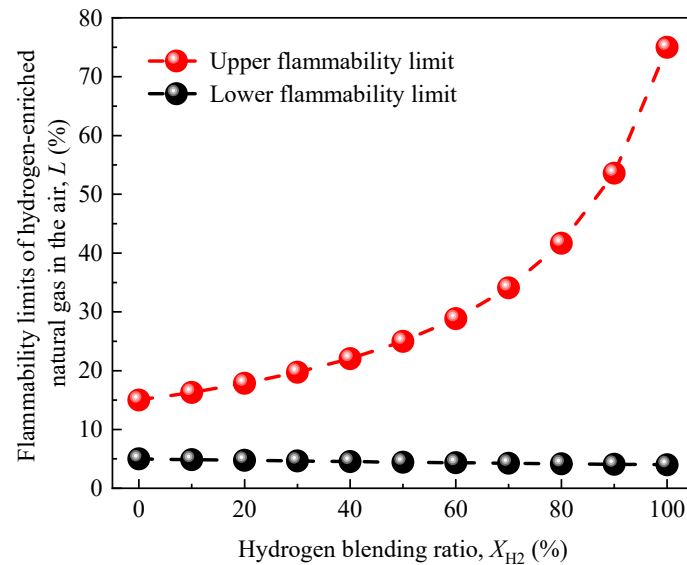


**Figure 3.** The variation in the flammability limits of hydrogen-enriched natural gas with different hydrogen blending ratios.

Figure 4 shows the variation in the ignition limits of hydrogen-enriched natural gas as the hydrogen blending ratio increases from 0% to 100%. The ignition limits, represented by the excess air ratio  $\lambda$ , can be obtained from the flammability limits according to Equation (3).

$$\lambda = \frac{1 - L}{\alpha L} \quad (3)$$

Here,  $\alpha$  denotes the theoretical air–fuel ratio of hydrogen-enriched natural gas. For methane,  $\alpha = 9.52$ , and for hydrogen,  $\alpha = 2.38$ .

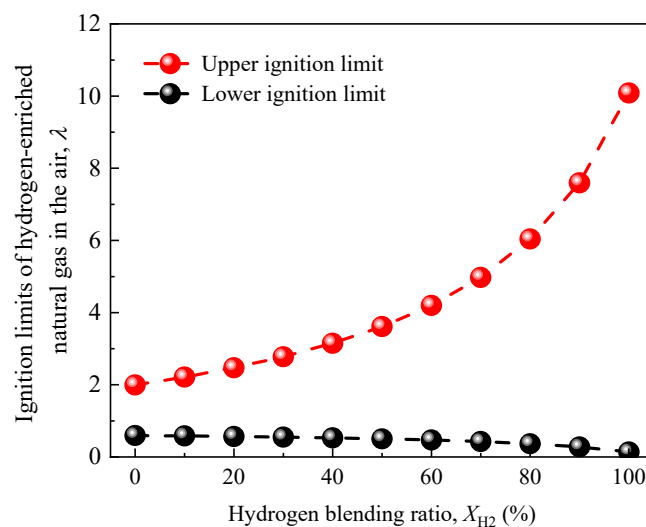


**Figure 4.** The variation in the ignition limits of hydrogen-enriched natural gas with different hydrogen blending ratios.

It can be seen from Figure 4 that the ignition limits of hydrogen-enriched natural gas gradually expand as the hydrogen blending ratio increases from 0% to 100%. Compared with pure methane (0.6–2), the ignition limits of hydrogen-enriched natural gas are closer to those of pure hydrogen (0.14–10) at a higher hydrogen blending ratio, implying that the ignition limits of the fuel can be effectively expanded by increasing the hydrogen blending ratio.

### 3. Field Experimental Tests and Chemical Reaction Network (CRN) Modeling Study

#### 3.1. Experimental and Modeling Setup

In this section, we discuss the 2 t/h gas-fired steam boiler that was used to carry out field experimental tests and to investigate the effects of the hydrogen blending ratio and excess air ratio on the boiler performance. The fuel and air flowed into the burner for combustion, and the generated flue gas flowed through the furnace and the post-heat exchange zone, finally exiting the boiler. As for the working fluid, the water was pumped into the boiler, heated to become steam, and finally delivered to the heat users. The boiler type is WNS2-1.25-Q, the rated saturated steam pressure is 1.25 MPa, the rated saturated steam temperature is 194 °C, and the other main operating parameters are listed in Table 5.

**Table 5.** Main operating parameters of gas-fired boiler.

Operating Parameters	Value	Operating Parameters	Value
Rated evaporation/(t/h)	2	Percentage of rated load/(%)	50
Feedwater pressure/(MPa)	0.1	Feedwater temperature/(°C)	25
Rated steam pressure/(MPa)	1.25	Rated steam temperature/(°C)	194
Inlet air and fuel pressure/(MPa)	0.1	Inlet air and fuel temperature/(°C)	15
Rated fuel flow rate/(m <sup>3</sup> /h)	70.2	Baseline oxygen content/(%)	3.5

The boiler in the field test is illustrated in Figure 5a and the hydrogen and natural gas blending plant is shown in Figure 5b. The steady-state operating time of the gas-fired boiler for each working condition is 40 min, the number of measurement readings are three, and the interval between two adjacent readings is 10 min.

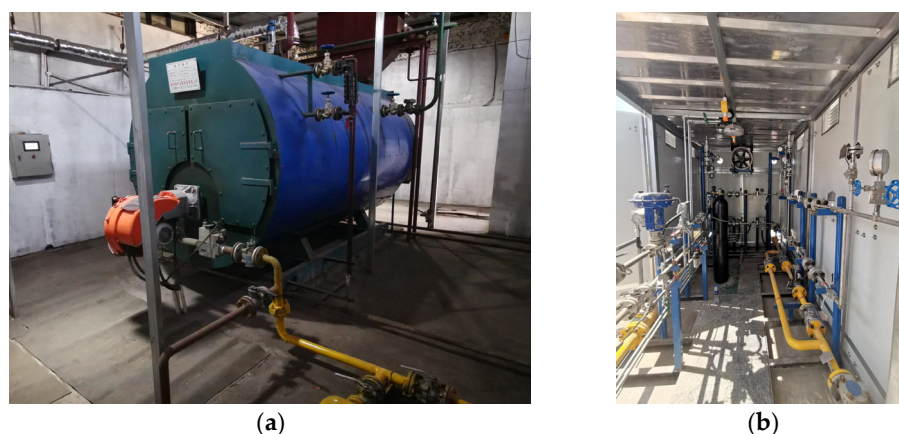


**Figure 5.** Pictures of (a) 2 t/h gas-fired steam boiler and (b) hydrogen and natural gas blending plant in field tests.

Due to the differences in the physicochemical properties of hydrogen and natural gas, the fuel properties of hydrogen-enriched natural gas vary with the hydrogen blending ratio. The fuel components used in the tests are listed in Table 6. The experiments focus on the lower heat value (LHV) of the fuel, in which the LHV of pure natural gas (Case 1) is 35.69 MJ/m<sup>3</sup>, the LHV of hydrogen-enriched natural gas with the hydrogen blending ratio of 9.7% (Case 2) is 33.19 MJ/m<sup>3</sup>, and the LHV of hydrogen-enriched natural gas with the hydrogen blending ratio of 10.1% (Case 3) is 33.09 MJ/m<sup>3</sup>. The LHV of hydrogen-enriched natural gas decreases with the increase in the hydrogen blending ratio.

**Table 6.** Fuel components and volume fractions.

Fuel Fabrication	Volumetric Fraction/(%)		
	Case 1	Case 2	Case 3
Methane	93.713	84.623	84.248
Ethane	4.573	4.129	4.111
Propane	1.084	0.979	0.975
Butane	0.255	0.230	0.229
Isobutane	0.265	0.239	0.238
n-Pentane	0.005	0.005	0.004
n-Pentane	0.010	0.009	0.009
2-Methylbutane	0.028	0.025	0.025
Nitrogen	0.067	0.061	0.060
Hydrogen sulfide	0.280	0.250	0.250
Saturated hydrocarbon	99.933	90.239	89.839

In the experimental process, the measured temperatures, pressures, flow rates, and flue gas components are detected by K-type thermocouples (Kaipusen Instruments Co. Ltd., Guangzhou, China), pressure sensors (Xingyi Sensor Manufacturing Co. Ltd., Beijing, China), turbine flowmeters (Sevenstar Flowmeter Co. Ltd., Beijing, China), and Testo 350 flue gas analyzers (Lenzkirch, Germany), respectively. Detailed information about the measuring instruments' ranges and accuracies has been provided in Table 7.

**Table 7.** Detailed information about measuring instruments.

Parameters	Measuring Instruments	Range	Accuracy *
$T$	K-type thermocouple	0–1100 °C	±1.5 °C
$p$	Pressure sensor	0–2 MPa	±0.5%
$V_{NG}$	Turbine flowmeter	0–150 m <sup>3</sup> /h	±0.5% MV
$V_{H2}$		0–50 m <sup>3</sup> /h	±0.5% MV
$V_{air}$		0–1500 m <sup>3</sup> /h	±1% MV
$O_2$	Testo 350	0–25%	±0.2%
$NO$		0–3000 ppm	±5% MV
$NO_2$		0–500 ppm	±5% MV
$CO$		0–10,000 ppm	±5% MV
$CO_2$		0–50%	±0.3% ± 0.1% MV
$SO_2$		0–5000 ppm	±5% MV

\* MV denotes the measured value.

According to Moffat's theory [28], the uncertainty of pollutant measurements  $\delta$  is calculated using Equation (4).

$$\delta = \sqrt{\beta^2 + (t_{0.95}(v)\sigma)^2} \quad (4)$$

Here,  $\beta$  denotes the accuracy of the Testo 350 flue gas analyzer (as shown in Table 7).  $\sigma$  denotes the standard deviation of the repeated pollutant measurements.  $t_{0.95}(v)$  denotes the student t value [29] with a confidence interval of 95%.

Moreover, based on the experimental data, the thermodynamic and heat transfer models of this boiler (WNS2-1.25-Q) were established to further study the thermodynamic characteristics at a higher hydrogen blending ratio of up to 30%. The control strategy of the operating parameters in this boiler after hydrogen addition is based on Scenario 2 in Wang's previous work [30], that is, the boiler heating load and control logic of the burner

remain constant. Under this circumstance, the fuel flow rate  $V_f$  is calculated according to Equation (5) to maintain the constant boiler heating load.

$$V_f = \frac{D_{sh} \times (I_{sh} - I_{fw})}{3.6 \times 1000 \times \eta_{th} \times LHV_f} \quad (5)$$

Here,  $D_{sh}$  denotes steam evaporation of the boiler, t/h.  $I_{sh}$  and  $I_{fw}$  denote the enthalpy of steam and feedwater, KJ/Kg.  $\eta_{th}$  denotes the boiler thermal efficiency, %.

The control logic of the burner is the fuel (the original natural gas) and air valve openings are preset in the one-to-one correspondence to keep an initial excess air ratio  $\lambda_{ini}$ . After hydrogen addition, the flow rate of hydrogen-enriched natural gas should be converted to the equivalent natural gas flow rate with the same fuel valve opening according to Equation (6).

$$V_{NG, eq} = \sqrt{\frac{\rho_f V_f^2}{\rho_{NG}}} \quad (6)$$

Here,  $\rho_f$  and  $\rho_{NG}$  denote the density of hydrogen-enriched natural gas and the original natural gas, kg/m<sup>3</sup>.

Then, the provided air flow rate can be obtained according to Equation (7).

$$V_{air} = 9.52 V_{NG, eq} \lambda_{ini} \quad (7)$$

Here,  $\lambda_{ini}$  denotes the initial excess air ratio when the fuel is natural gas, and the value is 1.23 here.

And the actual excess air ratio  $\lambda$  can be calculated by Equation (8).

$$\lambda = \frac{V_{air}}{4.76 \times (2 - 1.5X_{H_2}) V_f} \quad (8)$$

After obtaining the operating parameters of the boiler, the thermodynamic characteristics, such as theoretical combustion temperature, exhaust gas temperature, and boiler thermal efficiency, can be calculated based on the thermodynamic and heat transfer models of this boiler. A description of the aforementioned models can also be found in Wang's previous work [30], which is not to be described in detail here.

The Chemical Reactor Network (CRN) model is viewed as a fast and effective method for analyzing the pollutant emissions of gas-fired equipment [31]. Compared with the 3D computational fluid dynamic (CFD) approach, the CRN model approach is weak in depicting the spatial distribution of the parameters inside the boiler but very strong in the prediction of the variation in the chemical reactions using very detailed chemical kinetic mechanisms [32]. Additionally, the CRN model is favored in the present study due to its much faster computational speed compared to the 3D CFD simulation. The computational time for one case to simulate the pollutant emissions by the CRN model is generally less than 300 s. The solver algorithm employed automates coarse-to-fine grid refinement as a means to enhance the convergence in the calculation process. The maximum number of grid points allowed to solve the computational domain are 1000. The convergence criteria are absolute (ATOL) and relative (RTOL) tolerance used by the solver to determine convergence and absolute (ATLS) and relative (RTL) tolerance used by the solver to determine convergence for transient sensitivity coefficients. In this study, the values of ATOL, RTOL, ATLS, and RTL are set as  $10^{-9}$ ,  $10^{-6}$ ,  $10^{-6}$ , and  $10^{-4}$ , respectively. Once the calculation satisfies the convergence criteria, it is considered that the calculation is complete and the grid also completes its adaptive optimization.

In this study, the CRN model consisted of a perfectly stirred reactor (PSR) [33] and several plug flow reactors (PFRs) [34], and was also set up on the Chemkin Pro platform to assess the pollutant emissions of this boiler. As for the PSR model, it is a zero-dimensional model, and the reactants and the products are considered to be in a state of complete mixing

in the reactor, disregarding molecular transport and mixing processes; the mass and energy conservation equations are given in Equations (9) and (10).

$$m(Y_{k,\text{out}} - Y_{k,\text{in}}) - \omega_k M_k V_{\text{rea}} = 0 \quad (9)$$

$$m \sum_{k=1}^N (Y_{k,\text{out}} I_{k,\text{out}} - Y_{k,\text{in}} I_{k,\text{in}}) + Q_{\text{loss}} = 0 \quad (10)$$

Here,  $m$  denotes the mass flow rate, g/s.  $Y_{k,\text{in}}$  and  $Y_{k,\text{out}}$ , respectively, denote the mass fraction of the  $k$  component at the reactor inlet and outlet, %.  $\omega_k$  denotes the net production rate of the  $k$  component, mole/(cm<sup>3</sup>·s).  $M_k$  denotes the molar mass, g/mole.  $V_{\text{rea}}$  denotes the reactor volume, cm<sup>3</sup>.  $I_{k,\text{in}}$  and  $I_{k,\text{out}}$ , respectively, denote the enthalpy of the  $k$  component at the reactor inlet and outlet, erg/g.  $Q_{\text{loss}}$  denotes the heat loss of the reactor, erg/s.

The PFR model is one-dimensional, and the gas maintains a continuous steady flow; the continuity equation and the momentum, mass, and energy conservation equations are given in Equations (11)–(14).

$$\rho u \frac{dA}{dx} + \rho A \frac{du}{dx} + u A \frac{d\rho}{dx} = 0 \quad (11)$$

$$A \frac{dp}{dx} + \rho u A \frac{du}{dx} + \frac{dF}{dx} = 0 \quad (12)$$

$$\rho u \frac{dY_k}{dx} = M_k \omega_k \quad (13)$$

$$\rho u A \left( \sum_{k=1}^N I_k \frac{dY_k}{dx} + \bar{c}_p \frac{dT}{dx} + u \frac{du}{dx} \right) = Q_{\text{loss}} \quad (14)$$

Here,  $\rho$  denotes the gas density, g/cm<sup>3</sup>.  $u$  denotes the gas velocity, cm/s.  $A$  denotes the cross-sectional area of the reactor, cm<sup>2</sup>.  $p$  denotes the reactor pressure, dyn/cm<sup>2</sup>.  $F$  denotes the reactor wall forces, N.  $\bar{c}_p$  denotes the average constant-pressure specific heat in the reactor, erg/(g·K).

The schematic diagrams of the 2 t/h gas-fired steam boiler and its CRN model are shown in Figure 6. Given the structure of the triple-pass boiler, a combination of a PSR and a PFR represents the combustion and post-flame zone, which are solved using the energy conservation equation. The other two PFRs represent the furnace and the post-heat exchange zone, which are solved for a given flue gas temperature, and the flue gas temperature profile is obtained from the thermodynamic and heat transfer models.

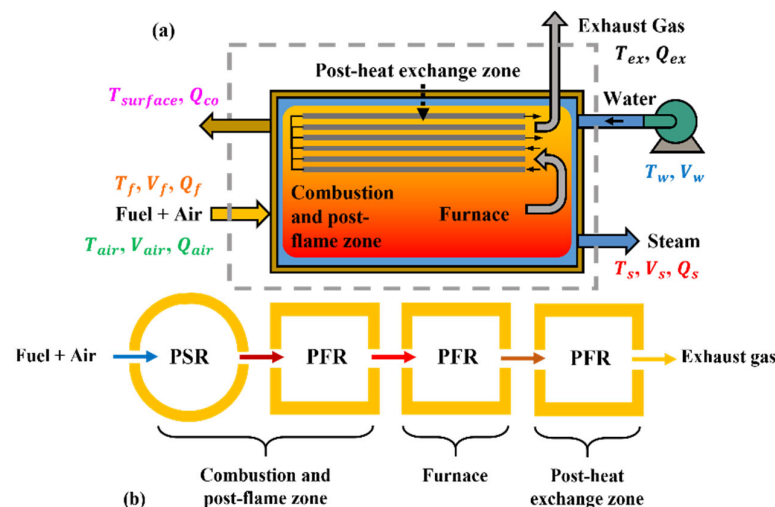


Figure 6. (a) Schematic diagram and (b) chemical reaction network model of boiler.

### 3.2. Boiler Performance Fueled with Hydrogen-Enriched Natural Gas

#### 3.2.1. Experimental Results and Discussion

The effects of the hydrogen blending ratio and excess air ratio on the thermal efficiency and pollutant emissions of the 2 t/h gas-fired steam boiler (WNS2-1.25-Q) of NDT Group Hydrogen Energy Company (Beijing, China) were experimentally investigated. Three tests with different hydrogen blending ratios were carried out. Specifically, they were Case 1 with a 0% hydrogen blending ratio (pure natural gas), Case 2 with a 9.7% hydrogen blending ratio, and Case 3 with a 10.1% hydrogen blending ratio. The tests were conducted following GB/T10180-2017 “Test Procedures for Thermal Performance of Industrial Boilers” [35], adopting the positive and negative balance methods to calculate the thermal efficiency of the boiler. The final results were based on the average of the positive balance efficiency and the negative balance efficiency. The detection indicators were determined according to TSG G0002-2010 “Supervision and Management Procedures for Energy Saving Technology of Boilers” [36]. Pollutant emissions were tested according to the “Beijing Boiler Air Pollutant Emission Standards” (DB 11/139-2015) for carbon monoxide, nitrogen oxide, and sulfur dioxide concentrations [37]. The test results of the three cases are shown in Table 8. It is worth mentioning that the tests were run under continuous and stable working conditions of the boiler system, during which the boiler combustion was stable, the equipment operated normally, and the main parameters remained stable.

**Table 8.** Boiler efficiency and pollutant emissions under various operating conditions.

Parameters	Case 1	Case 2	Case 3	Detection Indicators
Boiler evaporation/(t/h)	0.98	0.96	0.87	/
Vapor pressure/(MPa)	0.30	0.31	0.33	/
Exhaust heat loss $q_2$ /(%)	5.59	5.46	5.78	/
Cooling heat loss $q_5$ /(%)	5.92	6.04	6.67	/
Exhaust gas temperature $T_{ex}$ /(°C)	119.8	115.8	122.1	$\leq 170$
Excess air ratio at boiler exit $\lambda$	1.23	1.27	1.29	$\leq 1.15$
Thermal efficiency (positive) $\eta_1$ /(%)	89.42	88.78	86.90	/
Thermal efficiency (negative) $\eta_2$ /(%)	88.48	88.49	87.54	/
Average thermal efficiency $\eta_{1,2}$ /(%)	88.95	88.64	87.22	88
SO <sub>2</sub> /(mg/m <sup>3</sup> )	<3	<3	<3	/
NO <sub>x</sub> /(mg/m <sup>3</sup> )	118	112	125	/
CO/(mg/m <sup>3</sup> )	<1	<1	<1	/

From Table 5, it can be seen that the thermal efficiency of the 2 t/h gas-fired steam boiler is closely related to the exhaust heat loss and cooling heat loss, and the exhaust heat loss is largely determined by the exhaust gas temperature. As the hydrogen blending ratio increases from 0% to 9.7%, the excess air ratio in the furnace chamber increases from 1.23 to 1.27, and the exhaust heat loss decreases from 5.59% to 5.46%. However, the cooling heat loss increases from 5.92% to 6.04%, and thus, the overall thermal efficiency of the boiler shows a decreasing trend from 88.95% to 88.64%. As the hydrogen blending ratio increases from 9.7% to 10.1%, the excess air ratio in the furnace chamber increases from 1.27 to 1.29, and the exhaust heat loss also increases from 5.46% to 5.78%. Also, the cooling heat loss increases from 6.04% to 6.67%, and thus, the overall thermal efficiency of the boiler decreases from 88.64% to 87.22%. Generally, the fluctuation in the boiler thermal efficiency is within 1%.

The trend of NO<sub>x</sub> emissions is similar to that of the overall exhaust gas temperature of the boiler. As the hydrogen blending ratio increases from 0% to 9.7%, the exhaust gas temperature decreases from 119.8 °C to 115.8 °C, and the NO<sub>x</sub> emission decreases from 118 mg/m<sup>3</sup> to 112 mg/m<sup>3</sup>. As the hydrogen blending ratio increases from 9.7% to 10.1%, the exhaust gas temperature increases from 115.8 °C to 122.1 °C, and the NO<sub>x</sub> emission rises from 112 mg/m<sup>3</sup> to 125 mg/m<sup>3</sup>.

The CO and SO<sub>2</sub> emissions at the boiler exit meet the testing standards with and without hydrogen blending. CO emissions are all less than 1 mg/m<sup>3</sup>, and SO<sub>2</sub> emissions are all less than 3 mg/m<sup>3</sup>. From the above analysis, it can be seen that when the hydrogen blending ratio is less than 10%, compared with the non-hydrogen blending condition, the boiler thermal efficiency can be guaranteed while reducing the NO<sub>x</sub> emission by 5%.

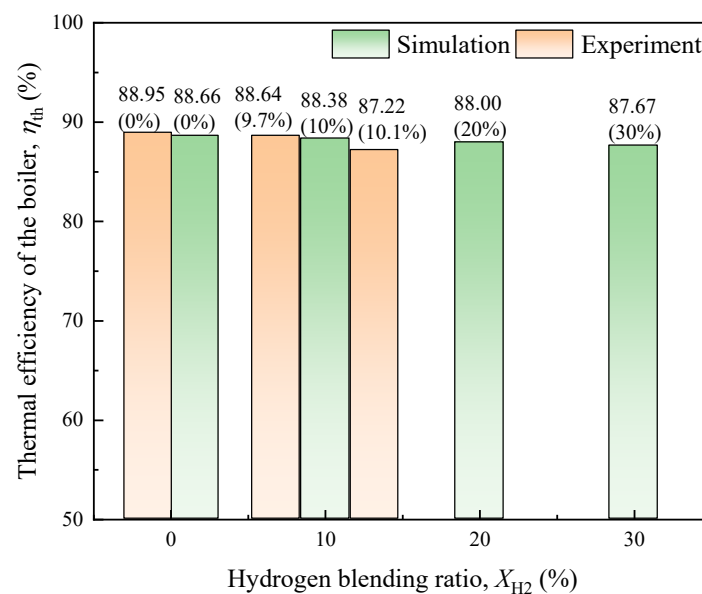
### 3.2.2. Modeling Results and Discussion

Table 9 shows the boiler heating load, volumetric flow rates of fuel and air, excess air ratio at the boiler exit, theoretical combustion temperature, and exhaust gas temperature under different hydrogen blending ratios. In the present study, the range of hydrogen blending ratios covers 0%-30% for operational safety considerations [11,23]. As  $X_{H_2}$  rises from 0% to 30%, the volumetric flow rate of fuel increases from 78.05 m<sup>3</sup>/h to 100.34 m<sup>3</sup>/h to maintain the constant boiler heating load. Also, the excess air ratio increases from 1.23 to 1.37, and the volumetric flow rate of air increases from 971.45 m<sup>3</sup>/h to 1070.55 m<sup>3</sup>/h. Moreover, the theoretical combustion temperature decreases from 1712 °C to 1597 °C due to the increase in excess air ratio after hydrogen addition, and the exhaust gas temperature increases from 120 °C to 130 °C.

**Table 9.** Boiler operating parameters and temperature profiles under different hydrogen blending ratios.

Parameters	$X_{H_2} = 0\%$	$X_{H_2} = 10\%$	$X_{H_2} = 20\%$	$X_{H_2} = 30\%$
Boiler evaporation/(t/h)	1	1	1	1
Volumetric flow rates of fuel $V_f$ /(m <sup>3</sup> /h)	78.05	84.34	91.69	100.34
Volumetric flow rates of air $V_{air}$ /(m <sup>3</sup> /h)	971.45	1002.29	1035.42	1070.55
Excess air ratio at boiler exit $\lambda$	1.23	1.27	1.32	1.37
Theoretical combustion temperature $T_{the}$ /(°C)	1712	1677	1635	1597
Exhaust gas temperature $T_{ex}$ /(°C)	120	123	127	130

Figures 7 and 8 illustrate the comparison of the boiler's thermal efficiency and the NO<sub>x</sub> emissions between the numerical simulation and field tests.



**Figure 7.** A comparison of the boiler's thermal efficiency between the simulation and experiments.

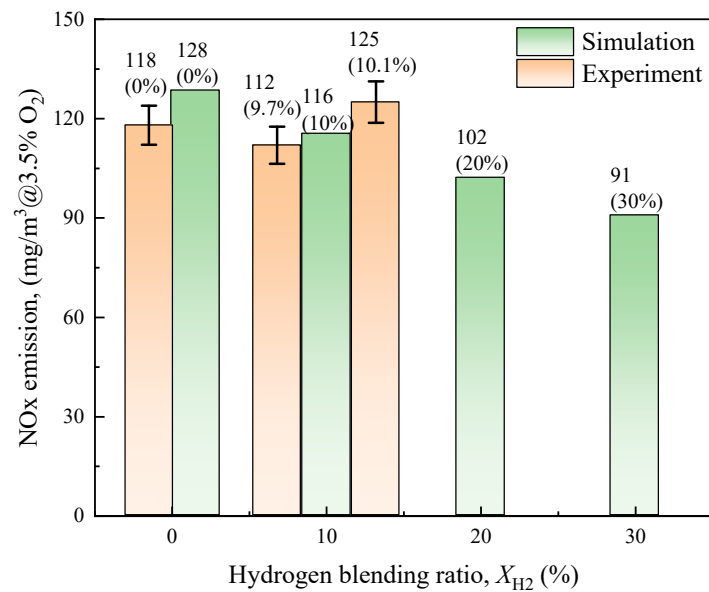


**Figure 8.** A comparison of the NOx emissions between the simulation and experiments.

The comparison indicates that the simulation and test results agree well, as the errors in boiler thermal efficiency are within  $\pm 1.5\%$ , and the errors in NOx emission are within  $\pm 10\%$ . As  $X_{H_2}$  rises from 0% to 30%, the boiler's thermal efficiency decreases from 88.66% to 87.67% as the exhaust heat loss increases. The NOx emission also decreases from 128 mg/m<sup>3</sup> to 91 mg/m<sup>3</sup> due to the decreased combustion temperature in the furnace. This means that increasing the excess air ratio after hydrogen addition benefits the inhibition of high temperatures in the furnace as well as NOx generation, but it also results in a decline in boiler thermal efficiency. There exists a tradeoff between NOx emission and boiler thermal efficiency in practice.

#### 4. Conclusions

The present study numerically investigated the combustion characteristics of hydrogen-enriched natural gas through the PREMIX model and OPPDOF model on the Chemkin Pro platform, focusing on the laminar flame propagation speed, extinction strain rate, and flammability limits of hydrogen-enriched natural gas under different hydrogen blending ratios and equivalence ratios. Subsequently, the combined investigation of field tests and modeling of a 2 t/h gas-fired steam boiler was conducted, and the effects of the hydrogen blending ratio and excess air ratio on the boiler's performance (e.g., boiler thermal efficiency, pollutant emissions, etc.) were studied. Specific conclusions include the following:

- (1) As the hydrogen blending ratio increases from 0% to 25%, the laminar flame propagation speed monotonically increases by 20.18%, 32.41%, and 30.18%, respectively, and the equivalence ratio equals 0.8, 1.0, and 1.2. The laminar flame propagation speed is more affected by hydrogen addition in fuel-rich combustion. In addition, the laminar flame propagation speed shows a trend of increasing and then decreasing as the equivalence ratio increases from 0.8 to 1.2. The laminar flame propagation speed at  $\Phi = 1.2$  is always higher than that at  $\Phi = 0.8$ , with the hydrogen blending ratio increasing from 0% to 25%.
- (2) Hydrogen addition expands the flammability limits of hydrogen-enriched natural gas, allowing it to maintain stable combustion in a leaner state. As the hydrogen blending ratio increases from 0% to 25%, the extinction strain rate monotonically increases by 81.18%, 59.13%, and 50.86%, respectively, and the equivalence ratio equals 0.8, 1.0, and 1.2. In addition, the extinction strain rate of the flame shows a trend of increasing and then decreasing as the equivalence ratio increases from 0.8 to 1.2. The extinction strain

- rate of the flame at  $\Phi = 1.2$  is always higher than that at  $\Phi = 0.8$ , with the hydrogen blending ratio increasing from 0% to 25%.
- (3) The field test results of a 2 t/h gas-fired steam boiler show that the simultaneous increase in the hydrogen blending ratio and excess air ratio makes the overall thermal efficiency of the boiler show a decreasing trend, but the fluctuation is within 1%. CO emissions are all less than  $1 \text{ mg/m}^3$ , and  $\text{SO}_2$  emissions are all less than  $3 \text{ mg/m}^3$ , which satisfies the test standards. As the hydrogen blending ratio increases from 0% to 9.7% and the excess air ratio increases from 1.23 to 1.27, the  $\text{NO}_x$  emission at the boiler exit decreases by 5% from  $118 \text{ mg/m}^3$  to  $112 \text{ mg/m}^3$ .
  - (4) According to the modeling results, as the hydrogen blending ratio increases from 0% to 30% and the excess air ratio simultaneously increases from 1.23 to 1.37, the theoretical combustion temperature in the furnace decreases from  $1712 \text{ }^\circ\text{C}$  to  $1597 \text{ }^\circ\text{C}$ , and the  $\text{NO}_x$  emission declines accordingly, from  $128 \text{ mg/m}^3$  to  $91 \text{ mg/m}^3$ . The exhaust gas temperature increases from  $120 \text{ }^\circ\text{C}$  to  $130 \text{ }^\circ\text{C}$ , and thus, the exhaust heat loss increases and the overall boiler thermal efficiency decreases from 88.66% to 87.67%. There exists a tradeoff between the  $\text{NO}_x$  emissions and the boiler's thermal efficiency in practice.

**Author Contributions:** Conceptualization, C.S., Y.L., W.L. and Y.Z. (Yang Zhang); methodology, T.W., P.W., Y.Z. (Yi Zhang) and Y.Z. (Yangxin Zhang); software, T.W. and Y.Z. (Yangxin Zhang); validation, Y.Z. (Yi Zhang) and C.C.; investigation, T.W., Y.Z. (Yi Zhang) and Y.Z. (Yangxin Zhang); writing—original draft, T.W., Y.Z. (Yi Zhang) and Y.Z. (Yangxin Zhang); writing—review and editing, C.S., P.W. and C.C.; supervision, Y.Z. (Yang Zhang); project administration, Y.L. and W.L.; funding acquisition, Y.L. and Y.Z. (Yang Zhang). All authors have read and agreed to the published version of the manuscript.

**Funding:** This research was funded by the Natural Science Foundation of China, grant number 52176116, and the Research Project of State Power Investment Corporation “Key Technology Research on Long-distance Hydrogen Mixing Transportation and Terminal Application of Natural Gas Pipeline”, grant number KYB12022QN02. The author Yang Zhang receives financial support from the Innovation Seed Fund of Shanxi Research Institute for Clean Energy, Tsinghua University.

**Data Availability Statement:** The authors will make the data available upon reasonable request.

**Conflicts of Interest:** Authors Chen Sun, Pengtao Wang, Chong Cui, Yanghui Lu and Wei Liu were employed by the company State Power Investment Corporation Research Institute Co., Ltd. The remaining authors declare that the research was conducted in the absence of any commercial or financial relationships that could be construed as a potential conflict of interest. The State Power Investment Corporation Research Institute Co., Ltd. had no role in the design of the study; in the collection, analyses, or interpretation of data; in the writing of the manuscript, or in the decision to publish the results.

## References

1. Luo, S.; Ma, F.; Mehra, R.K.; Huang, Z. Deep insights of HCNG engine research in China. *Fuel* **2020**, *263*, 116612. [[CrossRef](#)]
2. Rajhi, W.; Basem, A.; Sabri, L.S.; Mohammed, M.M.; Becheikh, N.; Kolsi, L.; Salahshour, S.; Al-Yasiri, M.; Sabetvand, R. A numerical study of catalytic combustion of methane-air in excess oxygen and deficient oxygen environments with increasing initial pressure: A molecular dynamic approach. *Case Stud. Therm. Eng.* **2024**, *57*, 104329. [[CrossRef](#)]
3. Hernandez-Gomez, R.; Tuma, D.; Lozano-Martin, D.; Chamorro, C.R. Accurate experimental ( $p, \rho, T$ ) data of natural gas mixtures for the assessment of reference equations of state when dealing with hydrogen-enriched natural gas. *Int. J. Hydrog. Energy* **2018**, *43*, 21983–21998. [[CrossRef](#)]
4. Tang, C.; Zhang, Y.; Huang, Z. Progress in combustion investigations of hydrogen enriched hydrocarbons. *Renew. Sust. Energy Rev.* **2014**, *30*, 195–216. [[CrossRef](#)]
5. Huang, Z.; Zhang, Y.; Zeng, K.; Liu, B.; Wang, Q.; Jiang, D. Measurements of laminar burning velocities for natural gas–hydrogen–air mixtures. *Combust. Flame* **2006**, *146*, 302–311. [[CrossRef](#)]
6. Dong, C.; Zhou, Q.; Zhang, X.; Zhao, Q.; Xu, T.; Hui, S. Experimental study on the laminar flame speed of hydrogen/natural gas/air mixtures. *Front. Chem. Eng. China* **2010**, *4*, 417–422. [[CrossRef](#)]
7. Miao, H.; Lu, L.; Huang, Z. Flammability limits of hydrogen-enriched natural gas. *Int. J. Hydrog. Energy* **2011**, *36*, 6937–6947. [[CrossRef](#)]

8. Oztarlik, G.; Selle, L.; Poinso, T.; Schuller, T. Suppression of instabilities of swirled premixed flames with minimal secondary hydrogen injection. *Combust. Flame* **2020**, *214*, 266–276. [[CrossRef](#)]
9. Hu, Z.; Zhang, X. Study on laminar combustion characteristic of low calorific value gas blended with hydrogen in a constant volume combustion bomb. *Int. J. Hydrog. Energy* **2019**, *44*, 487–493. [[CrossRef](#)]
10. Ghosh, A.; Munoz-Munoz, N.M.; Lacoste, D.A. Minimum ignition energy of hydrogen-air and methane-air mixtures at temperatures as low as 200 K. *Int. J. Hydrog. Energy* **2022**, *47*, 30653–30659. [[CrossRef](#)]
11. Colorado, A.; McDonell, V. Surface stabilized combustion technology: An experimental evaluation of the extent of its fuel-flexibility and pollutant emissions using low and high calorific value fuels. *Appl. Therm. Eng.* **2018**, *136*, 206–218. [[CrossRef](#)]
12. Griebel, P.; Boschek, E.; Jansohn, P. Lean blowout limits and NO<sub>x</sub> emissions of turbulent, lean premixed, hydrogen-enriched methane/air flames at high pressure. *J. Eng. Gas Turbines Power* **2007**, *129*, 404–410. [[CrossRef](#)]
13. Lo Basso, G.; Nastasi, B.; Garcia, D.A.; Cumo, F. How to handle the hydrogen enriched natural gas blends in combustion efficiency measurement procedure of conventional and condensing boilers. *Energy* **2017**, *123*, 615–636. [[CrossRef](#)]
14. Hoelzner, K.; Szyszka, A. Operation of 20 kW<sub>th</sub> gas-fired heating boilers with hydrogen, natural gas and hydrogen/natural gas mixtures. First test results from Phase 1 (March 1993) of the Neunburg Vorm Wald solar hydrogen project. *Int. J. Hydrog. Energy* **1994**, *19*, 843–851. [[CrossRef](#)]
15. Ding, Y.; Durox, D.; Darabiha, N.; Schuller, T. Chemiluminescence based operating point control of domestic gas boilers with variable natural gas composition. *Appl. Therm. Eng.* **2019**, *149*, 1052–1060. [[CrossRef](#)]
16. Öztuna, S.; Büyükkakın, M.K. Effects of hydrogen enrichment of methane on diffusion flame structure and emissions in a back-pressure combustion chamber. *Int. J. Hydrog. Energy* **2020**, *45*, 5971–5986. [[CrossRef](#)]
17. Wang, T.; Liu, X.; Zhang, Y.; Zhang, H. Thermodynamic and emission characteristics of a hydrogen-enriched natural gas-fired boiler integrated with external flue gas recirculation and waste heat recovery. *Appl. Energy* **2024**, *358*, 122614. [[CrossRef](#)]
18. Schiro, F. Research and Development of Premixed Burners, with Particular Attention to the Emissions, the Modulation Range and the Ability to Work Efficiently with Different Fuel Gases. Ph.D. Thesis, University of Padova, Padova, Italy, 2017.
19. Schiro, F.; Stoppato, A.; Benato, A. Modelling and analyzing the impact of hydrogen enriched natural gas on domestic gas boilers in a decarbonization perspective. *Carbon Resour. Convers.* **2020**, *3*, 122–129. [[CrossRef](#)]
20. Bălănescu, D.T.; Homutescu, V.M. Effects of hydrogen-enriched methane combustion on latent heat recovery potential and environmental impact of condensing boilers. *Appl. Therm. Eng.* **2021**, *197*, 117411. [[CrossRef](#)]
21. Celtek, M.S.; Pınarbaşı, A. Investigations on performance and emission characteristics of an industrial low swirl burner while burning natural gas, methane, hydrogen-enriched natural gas and hydrogen as fuels. *Int. J. Hydrog. Energy* **2018**, *43*, 1194–1207. [[CrossRef](#)]
22. Büyükkakın, M.K.; Öztuna, S. Numerical investigation on hydrogen-enriched methane combustion in a domestic back-pressure boiler and non-premixed burner system from flame structure and pollutants aspect. *Int. J. Hydrog. Energy* **2020**, *45*, 35246–35256. [[CrossRef](#)]
23. Jones, D.R.; Al-Masry, W.A.; Dunnill, C.W. Hydrogen-enriched natural gas as a domestic fuel: An analysis based on flash-back and blow-off limits for domestic natural gas appliances within the UK. *Sustain. Energy Fuels* **2018**, *2*, 710–723. [[CrossRef](#)]
24. Ansys, Inc. Ansys Chemkin-Pro Theory Manual. Canonsburg, PA, USA, 15317. Available online: <http://www.ansys.com> (accessed on 1 January 2019).
25. Smith, G.P.; Tao, Y.; Wang, H. Foundational Fuel Chemistry Model Version 1.0 (FFCM-1). 2016. Available online: <http://nanoenergystanfordedu/ffcm1> (accessed on 17 October 2020).
26. Yang, X.; Wang, T.; Zhang, Y.; Zhang, H.; Wu, Y.; Zhang, J. Hydrogen effect on flame extinction of hydrogen-enriched methane/air premixed flames: An assessment from the combustion safety point of view. *Energy* **2022**, *239*, 122248. [[CrossRef](#)]
27. ISO/FDIS 14532,2001(E/F); Natural Gas–Vocabulary. ISO: Geneva, Switzerland, 2001.
28. Moffat, R.J. Describing the uncertainties in experimental result. *Exp. Therm. Fluid Sci.* **1988**, *1*, 3–17. [[CrossRef](#)]
29. Brereton, R.G. The t-distribution and its relationship to the normal distribution. *J. Chemometr.* **2015**, *29*, 481–483. [[CrossRef](#)]
30. Wang, T.; Zhang, H.; Zhang, Y.; Wang, H.; Lyu, J.; Yue, G. Efficiency and emissions of gas-fired industrial boiler fueled with hydrogen-enriched nature gas: A case study of 108 t/h steam boiler. *Int. J. Hydrog. Energy* **2022**, *47*, 28188–28203. [[CrossRef](#)]
31. Colorado, A.; McDonell, V. Emissions and stability performance of a low-swirl burner operated on simulated biogas fuels in a boiler environment. *Appl. Therm. Eng.* **2018**, *130*, 1507–1519. [[CrossRef](#)]
32. Benedetto, D.; Pasini, S.; Falcitelli, M.; Marca, C.L.; Tognotti, L. NO<sub>x</sub> emission prediction from 3-D complete modelling to reactor network analysis. *Combust. Sci. Technol.* **2000**, *153*, 279–294. [[CrossRef](#)]
33. Rutar, T.; Malte, P.C. Nox formation in high-pressure jet-stirred reactors with significance to lean-premixed combustion turbines. *J. Eng. Gas Turb. Power* **2002**, *124*, 776–783. [[CrossRef](#)]
34. Kang, Y.; Lu, X.; Wang, Q.; Ji, X.; Miao, S.; Zong, C.; Luo, G.; Liu, H. An experimental and modeling study of NO<sub>x</sub> and CO emission behaviors of dimethyl ether (DME) in a boiler furnace. *Fuel Process. Technol.* **2014**, *122*, 129–140. [[CrossRef](#)]
35. GB/T10180-2017; Thermal Performance Test Code for Industrial Boilers. Standardization Administration of China: Beijing, China, 2017.

36. *TSG G0002-2010*; Supervision Administration Regulation on Energy Conservation Technology for Boiler. General Administration of Quality Supervision, Inspection and Quarantine of the People's Republic of China: Beijing, China, 2010.
37. *DB 11/139-2015*; Emission Standard of Air Pollutants for Boilers. Beijing Municipal Administration of Quality and Technology Supervision and Beijing Municipal Environmental Protection Bureau: Beijing, China, 2015.

**Disclaimer/Publisher's Note:** The statements, opinions and data contained in all publications are solely those of the individual author(s) and contributor(s) and not of MDPI and/or the editor(s). MDPI and/or the editor(s) disclaim responsibility for any injury to people or property resulting from any ideas, methods, instructions or products referred to in the content.